



HAL
open science

Improved Creep Resistance at 1000°C of a Medium Entropy Alloy by the In Situ Formation of Intergranular MC Carbides

Corentin Gay, Nassima Chenikha, Pauline Spaeter, Erwan Etienne, A. Vernière, Lionel Aranda, Patrice Berthod

► To cite this version:

Corentin Gay, Nassima Chenikha, Pauline Spaeter, Erwan Etienne, A. Vernière, et al.. Improved Creep Resistance at 1000°C of a Medium Entropy Alloy by the In Situ Formation of Intergranular MC Carbides. Indonesian Journal of Innovation and Applied Sciences (IJIAS), 2024, 4 (2), pp.141-149. 10.47540/ijias.v4i2.971 . hal-04646995

HAL Id: hal-04646995

<https://hal.science/hal-04646995>

Submitted on 12 Jul 2024

HAL is a multi-disciplinary open access archive for the deposit and dissemination of scientific research documents, whether they are published or not. The documents may come from teaching and research institutions in France or abroad, or from public or private research centers.

L'archive ouverte pluridisciplinaire **HAL**, est destinée au dépôt et à la diffusion de documents scientifiques de niveau recherche, publiés ou non, émanant des établissements d'enseignement et de recherche français ou étrangers, des laboratoires publics ou privés.



Distributed under a Creative Commons Attribution - ShareAlike 4.0 International License



Volume 4	Issue 2	June (2024)	DOI: 10.47540/ijias.v4i2.971	Page: 141 – 149
----------	---------	-------------	------------------------------	-----------------

Improved Creep Resistance at 1000°C of a Medium Entropy Alloy by the In Situ Formation of Intergranular MC Carbides

Corentin Gay¹, Nassima Chenikha¹, Pauline Spaeter¹, Erwan Etienne¹, Anne Vernière¹, Lionel Aranda¹, Patrice Berthod¹

¹Institut Jean Lamour, Université de Lorraine, France

Corresponding Author: Patrice Berthod; Email: patrice.berthod@univ-lorraine.fr

ARTICLE INFO

Keywords: Creep Resistance, High Temperature, Medium Entropy Alloy, Thermal Analysis.

Received : 23 June 2023

Revised : 22 Agustus 2023

Accepted : 29 June 2024

ABSTRACT

A Cantor's alloy with modified contents in manganese and chromium, elaborated by classical foundry, was enriched either in tantalum and carbon or in hafnium and carbon, to promote the formation of MC carbides to try improving the poor creep resistance of the original quinary alloy for possible use at 1000°C. Similarly to what was observed in recent investigations, metallography allowed checking that interdendritic/intergranular MC carbides were obtained here too. The two monocarbides-containing alloys were first subjected to differential thermal analysis to specify notably their melting start temperatures, to validate the chosen temperature for the creep tests. Three-point flexural creep tests were then performed at 1000°C, which indisputably demonstrated the outstanding strengthening effect of these MC carbides for the modified Cantor's alloy.

INTRODUCTION

Many high-temperature applications require metallic materials with long lifetimes for working under significant constant or variable stresses in contact with chemically aggressive fluids, and gas mixtures (from dry or wet air to combustion gases). The superalloys developed for more than half of a century now satisfactorily respond to these needs (Bradley, 1988; Donachie & Donachie, 2002; Sims & Hagel, 1972) do to their well-designed microstructures but their chemical compositions are too rich either in nickel (Balikci & Altincekic, 2019; Semiatin et al., 2017; Zhao, 2014) or in cobalt (Gui et al., 2019; Liu et al., 2020; Wei et al., 2015) to guarantee independence of these elements which are more and more considered as critical since a couple of decades (Ilyas et al., 2022; Kriese et al., 2023; Lughofer & Tost, 2023). With the exponentially increasing interest in High Entropy Alloys (HEA) (Asadikiya et al., 2022; Cantor, 2021; Firstov et al., 2016; Razumov et al., 2023) for various types of applications whatever the conditions of use, one can imagine decreasing the cobalt and nickel contents by introducing metals

with similar molar masses and properties but much more abundant and cheaper. New elements to add can be thus iron (Chen et al., 2015; Li et al., 2023; Yin et al., 2020) and manganese (Anzini et al., 2020; Lu et al., 2021; Pedrazzini et al., 2016). A now rather old HEA, Cantor's alloy (Cantor, 2021; Oliveros et al., 2021; Smekhova et al., 2023), can be considered as corresponding to such partial replacement of Ni and Co by Fe and Mn. Unfortunately, the mechanical behavior of this equimolar CoNiFeMnCr alloy, which is of high interest for temperatures not too high down to cryogenic temperatures (Ji & Wu, 2022; Oliveros et al., 2021; Thurston et al., 2017), becomes disappointing at high temperatures (Chen et al., 2023). It was recently tested to reinforce it by MC carbides (Berthod, 2023a) which are both remarkably efficient for strengthening cast Al-free/Cr-containing Ni-based (Li et al., 2014; Li et al., 2015; Sun et al., 2015; Qin et al., 2023) and Co-based (Barajas-Alvarez et al., 2022; Chang & Chen, 2014a; Chang & Chen, 2014b; Gui et al., 2017; Jafari et al., 2018) alloys and highly stable at elevated temperature. These TaC-reinforced and HfC-

reinforced equimolar CoNiFeMnCr-based cast alloys demonstrated enhanced creep-resistance at temperatures up to 1100°C (Berthod, 2023a). Unfortunately, the oxidation behavior at high temperatures of these MC-reinforced HEAs was of the same type as the base alloy one, i.e. poor enough not to allow taking benefit from the good high-temperature mechanical properties (Berthod, 2023b). This can be due first to the little too low chromium content – considering that 20 wt.% is the strict minimum for a Ni-based alloy while this threshold goes up to 30 wt.% for a Co-based one (Kofstad, 1988; Young, 2008) – and second to the particular behavior of manganese which was observed. It was thereafter decided to modify the contents of these two elements. Three alloys, two MC-strengthened ones (+ 0.25C and 3.7Ta or Hf), and a carbide-free one for comparison, were thus designed and elaborated [14]. These CoNiFeMn_{0.5}Cr_{1.5}-based alloys (with Mn contents divided by 2 and Cr contents increased by 50%) were preliminarily metallographically characterized to explore their as-cast microstructures (still identical to the carbide-free or -containing equimolar alloy's ones). The purpose of the present work is to test them in 3 points of flexural creep to check if their high-temperature creep resistance was not affected by these changes, before their characterization in oxidation at high temperature.

METHODS

Alloys

The chemical composition of the alloy, as measured during the chemical and metallographic characterization of the as-cast alloys [14] is reminded in Table 1 for the carbide-free CoNiFeMn_{0.5}Cr_{1.5} alloy (base alloy, new reference alloy), Table 2 for the TaC-containing alloy and Table 3 for the HfC-containing alloy. Since their bases are non-equimolar, as significantly Mn-impoverished and Cr-enriched versions of the initial HEAs [9,10], it is convenient to give them names based on MEA (Medium Entropy Alloys), as is to say: “MEA” (for the non-equimolar quinary alloy), “MEA/TaC” for the one containing tantalum monocarbides and “MEA/HfC” for the one containing hafnium monocarbides.

The as-cast microstructures of these alloys are reminded in Figure 1 for the MEA alloy, in Figure 2 for the MEA/TaC alloy, in Figure 3 for the

MEA/HfC alloy. The MEA alloy is single-phased (austenitic, Face Centered Cubic network), while the MEA/TaC and MEA/HfC alloys are double-phased {FCC matrix, TaC or HfC}, as earlier evidenced by X-Ray Diffraction (XRD) [9,10]. Elemental EDS mapping revealed that the MEA alloy and the matrixes of the MEA/TaC and MEA/HfC alloys were not really homogeneous chemically because of Mn enrichment of the peripheral part of the solidification cells (the MEA alloy) or of the solidification dendrites (the MEA/TaC and MEA/HfC alloys) [9,10]. These Mn segregations that occurred during solidification were logically more efficiently more evidenced in the single-phased alloys than in the two other alloys in which they tended to be partly hindered by the eutectic carbides locally precipitated at the end of solidification.

Table 1. Compositions of the carbide-free alloy (average and standard deviation from 5 full frame ×250 Energy Dispersion Spectrometry analyses)

MEA Full			
Frame (wt.%)	Co	Ni	Fe
Average	20.0	20.5	19.8
Standard Deviation	0.1	0.3	0.18
	Mn	Cr	M
	8.3	31.3	/
	0.5	0.4	/

Table 2. Compositions of the TaC-containing alloy (average and standard deviation from 5 full frame ×250 Energy Dispersion Spectrometry analyses)

MEA/TaC			
Full Frame (wt.%)	Co	Ni	Fe
Average	19.5	20.0	19.1
Standard Deviation	0.2	0.5	0.3
	Mn	Cr	Ta
	8.4	28.5	4.6
	0.2	0.3	0.2

Table 3. Compositions of the TaC-containing alloy (average and standard deviation from 5 full frame $\times 250$ Energy Dispersion Spectrometry analyses)

MEA/HfC			
Full Frame (wt.%)	Co	Ni	Fe
Average	19.7	20.1	19.1
Standard Deviation	0.4	0.3	0.3
	Mn	Cr	Hf
	8.8	27.8	4.5
	0.3	0.7	0.6

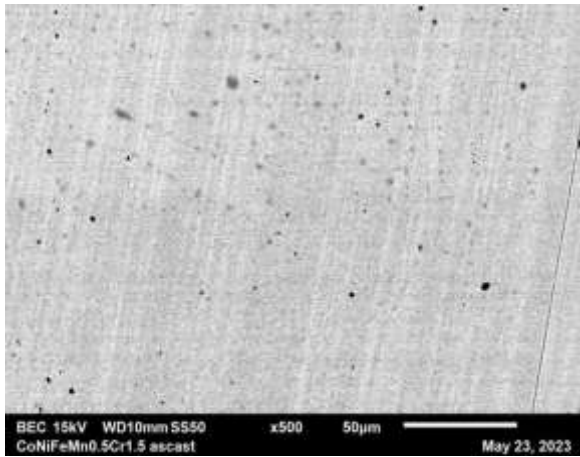


Figure 1. Back Scattered Electrons image of the microstructure of the MEA alloy (CoNiFeMn_{0.5}Cr_{1.5})

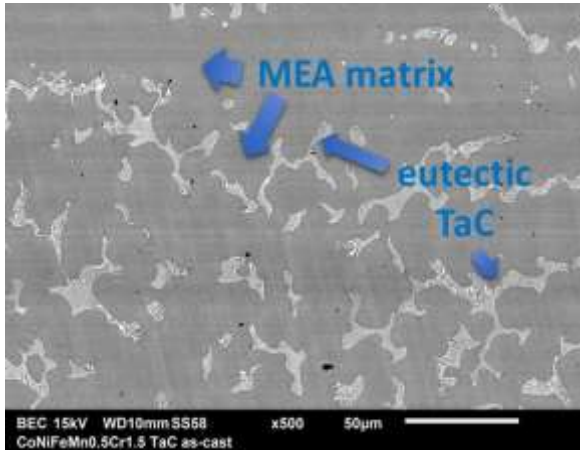


Figure 2. Back Scattered Electrons image of the microstructure of the MEA/TaC alloy (MEA+0.25C+3.7Ta, wt.%)

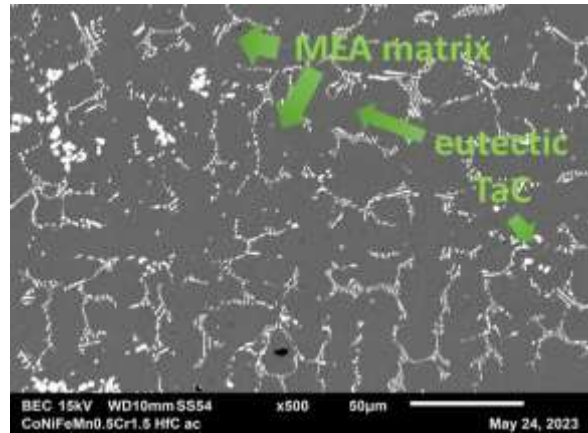


Figure 3. Back Scattered Electrons image of the microstructure of the MEA/HfC alloy (MEA+0.25C+3.7Hf, wt.%)

The samples for the creep tests were machined in the same ingots as the samples for the microstructure characterizations [9,10].

Creep Tests

The creep behaviors of the three alloys at high temperatures were investigated according to the centered 3-point flexural method illustrated in Figure 4. A parallelepiped cut in the ingot using a metallography precision saw (shape and examples of dimensions given in Figure 5) was placed on two 12 mm spaced parallel alumina rods playing the roles of the two bottom supports. A long third alumina rod cut in “V” at its extremity was placed as the top point and a charge of several hundred grams (accurately rated to obtain a maximal stress of 20 MPa at the middle of the bottom of the parallelepiped sample (Figure 6). The heating up to 1000°C was then achieved, at +20°C/min. The displacement of the top contact point was recorded during the heating and the isothermal stage but time and displacement were reinitialized at 0 at the beginning of the isothermal stage. The results were plot versus time only for the isothermal part.

Flexural centered 3 points loading mode

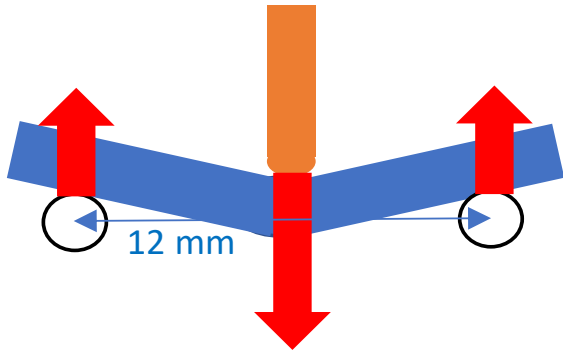


Figure 4. The principle of using the creep test

Dimensions of the parallelepiped creep samples

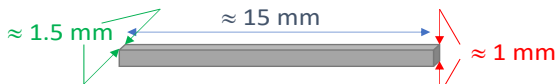


Figure 5. Typical dimensions of the parallelepiped samples

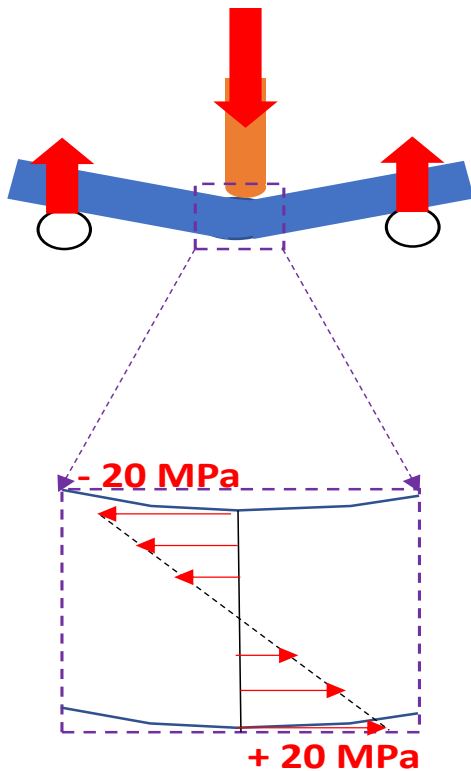


Figure 6. Induced linear distribution of stress between compression (top half of the sample) and traction (bottom half); location of the 20 MPa maximal tensile stress in the middle of the bottom

RESULTS AND DISCUSSION

Creep Behavior of the MEA Alloy

At 1000°C under a central load inducing a maximal local tensile stress equal to 20 MPa, the MEA sample deformed rapidly (Figure 7), with about 200 μm per 10 hours in the second creep stage (called steady state). The main part of the primary stage was obviously already achieved when arriving at the start of the isothermal part of the test. The third creep stage led to contact with the alumina basis in less than 5 hours. Plotting, versus time, the deformation rate instead of the deformation itself (Figure 8), allows better distinguishing the second creep stage (constant rate) from the first one (deceleration) and the third one (final acceleration), and also specifying the steady state deformation rate: close to 20 μm/h.

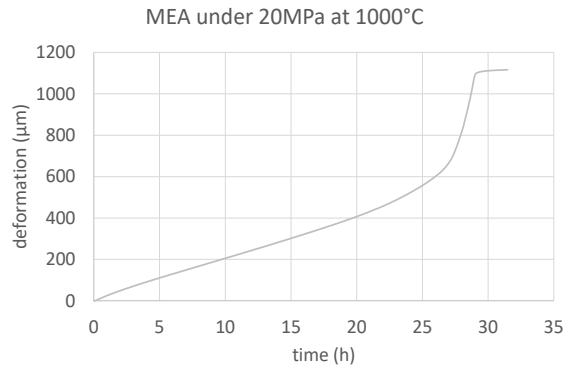


Figure 7. Central point displacement versus time for the MEA alloy

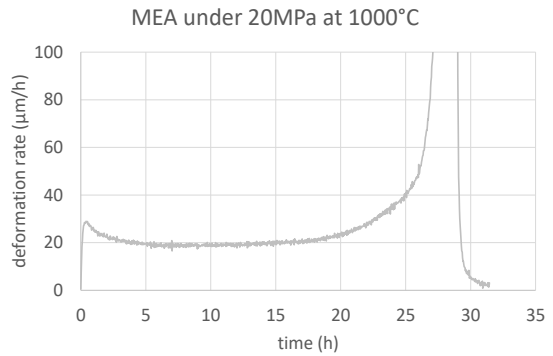


Figure 8. Central point displacement rate versus time for the MEA alloy

The MEA sample after the creep test was photographed (Figure 9). No rupture occurred of course (rare during 3-point bending tests), but the sample appears as being visco-plastically very deformed.

MEA 20MPa 1000°C ≈ 24h



Figure 9. Photograph of the MEA alloy sample after the creep test

Creep of the MEA/TaC Alloy

The deformation curve obtained for the MEA/TaC alloy presents a very different shape by comparison with the MEA alloy (Figure 10). The first creep stage (consolidation, progressive deceleration of deformation), probably started during the heating, was far from being finished when the temperature reached the isothermal one, and went on for about 25 hours. The second creep stage began late and was not finished when the test was interrupted. In addition, the constant rate during this steady state creep deformation was very low (Figure 11) by comparison with the carbide-free MEA alloys, and the sample after the test was only a little deformed (Figure 12). In the deformation curve (Figure 10), one must notice a small jump between 60 and 70 hours, but the deformation became again very slow thereafter. At 90 hours of the isothermal stage, the total deformation was less than only 70µm.

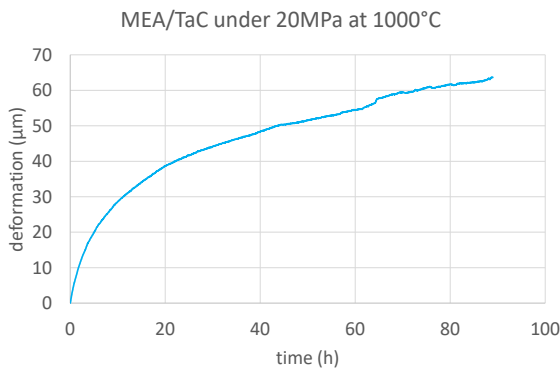


Figure 10. Central point displacement versus time for the MEA/TaC alloy

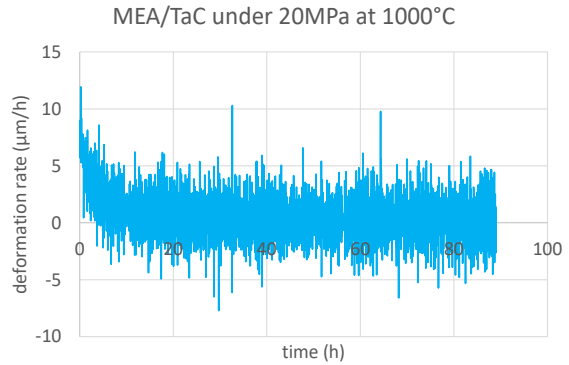


Figure 11. Central point displacement rate versus time for the MEA/TaC alloy

MEA/TaC 20MPa 1000°C > 90h



Figure 12. Photograph of the MEA/TaC alloy sample after the creep test

Creep of the MEA/HfC Alloy

The MEA/HfC alloy behaved similarly to the MEA/TaC one, as illustrated by Figure 13, Figure 14, and Figure 15: a significant part of the primary creep stage isothermally made, a very low steady-state deformation rate, and a post-test sample almost not deformed. In its case, no small jump occurred during the steady state deformation.

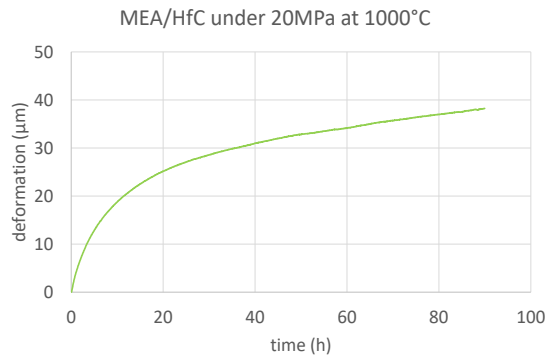


Figure 13. Central point displacement versus time for the MEA/HfC alloy

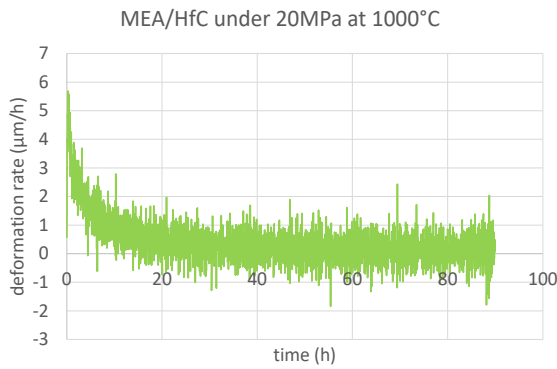


Figure 14. Central point displacement rate versus time for the MEA/HfC alloy

MEA/HfC 20MPa 1000°C > 90h



Figure 15. Photograph of the MEA/HfC alloy sample after the creep test

Comparison Between the Three Alloys

To visualize globally the differences in creep behavior between, on one hand, the MEA alloy and on the other hand the MEA/TaC and MEA/HfC alloys, the three curves are plotted together in the same graph in Figure 16. The characteristics of the curves are gathered in Table 4.

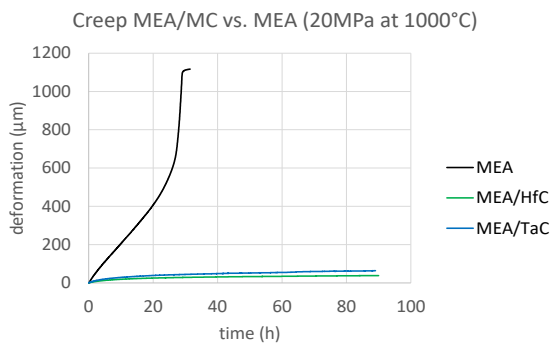


Figure 16. The three {central point displacement versus time} curves

Table 4. Values of several parameters characterizing the creep deformation curves

Alloys	First Creep Stage	
	Duration	Deformation
MEA	6h	128µm
MEA/TaC	25h	42µm
MEA/HfC	30h	29µm
Second Creep Stage		
	Duration	Derform.rate
	14h	20µm/h
	>90h	0.22µm/h
	>90h	0.13µm/h
Third Creep Stage		
	Duration to contact base	
	9h	
	Not reached	
	Not reached	

The most interesting data in this table are certainly the values of the constant deformation rates measured during the steady state creep: the deformation rates of the carbide-containing alloys are 100 times lower than the carbide-free alloys one.

CONCLUSION

It appeared thus clear, in this study, that the presence of either TaC or HfC carbides considerably strengthens the CoNiFeMn_{0.5}Cr_{1.5} alloy as they did for its initial equimolar version (Chen et al., 2023). Mechanically, the MEA/TaC and MEA/HfC are good for service at 1000°C. However, this needs to be confirmed for other stress levels. These additional creep tests are scheduled after the ongoing oxidation tests which can be reasonably expected to demonstrate significant improvements from the poor oxidation behaviors observed for the initial (Co, Ni, Fe, Mn, Cr)-equimolar versions of these alloys (Berthod, 2023b), thanks to the increase of the Cr content to about 30 wt.%Cr which ought to be sufficient. However, in case of disappointing results about the high-temperature oxidation behavior of these Mn-poorer Cr-richer alloys, it will be possible to totally remove Mn from the composition with or without replacement by a new element. This one can be Cu for instance, since copper is present in some HEA alloys (Bürckner et al., 2023; Campo et al., 2021; Galetz et al., 2021; Gwalani et al., 2019; Mukanov

et al., 2023). Al can be also usefully considered (Asadikiya et al., 2022; Kaypour et al., 2023; Sathyanarayana et al., 2018), taking into account the well-known beneficial influence of this element on the oxidation behavior at high temperature.

REFERENCES

1. Anzini, E., Glaenger, N., Mignanelli, P.M., Hardy, M.C., Stone, H.J., Pedrazzini, S. (2020). The effect of manganese and silicon additions on the corrosion resistance of a polycrystalline nickel-based superalloy. *Condensed Matter*, 1-21.
2. Asadikiya, M., Zhang, Y., Wang, L., Apelian, D., Zhong, Y. (2022). Design of ternary high-entropy aluminum alloys (HEAs). *Journal of Alloys and Compounds*, 891: 161836.
3. Balikci, E., Altincekic, A. (2019). Fine precipitates in nickel base superalloys. *Journal of Material Science and Technology Research*, 6: 1-8.
4. Barajas-Alvarez, M.R., Bedolla-Jacuinde, A., Lopez-Morelos, V.H., Ruiz, A. (2022). Creep behavior and microstructural characterization of cobalt-based superalloy. *MRS Advances*, 7: 1109-1114.
5. Berthod, P. (2023a). Strengthening against Creep at Elevated Temperature of HEA Alloys of the CoNiFeMnCr Type Using MC-Carbides, In: *Supplemental Proceedings to the TMS 2023 Annual Meeting & Exhibition* (San Diego): 1103-1111.
6. Berthod, P. (2023b). High Temperature Oxidation of CoNiFeMnCr High Entropy Alloys Reinforced by MC-Carbides, In: *Supplemental Proceedings to the TMS 2023 Annual Meeting & Exhibition* (San Diego): 933-941.
7. Bradley, E.F. (1988). *Superalloys: A Technical Guide*, ASM International, Metals Park.
8. Bürckner, M.L.; Mengis, L., White, E.M.H., Galetz, M.C. (2023). Influence of copper and aluminum substitution on high-temperature oxidation of the FeCoCrNiMn “Cantor” alloy. *Materials and Corrosion*, 74:79-90.
9. Campo, K.N., de Freitas, C.C.; da Fonseca, E.B., Caram, R. (2021). CrCuFeMnNi high-entropy alloys for semisolid processing: The effect of copper on phase formation, melting behavior, and semisolid microstructure. *Materials Characterization*, 178:111260.
10. Cantor, B. (2021). Multicomponent high-entropy Cantor alloys. *Progress in Materials Science*, 120: 100754.
11. Chang, S.H., Chen, C.C. (2014a). The effects of HIP, solution heat treatment and aging treatments on the microstructure and mechanical properties of sintering cobalt-based alloys strengthened with tantalum carbide additives. *Materials Transactions*, 55: 1755-1761.
12. Chang, S.H.; Chen, C.C. (2014b). Microstructure and mechanical properties of cobalt-based alloys strengthened with tantalum carbide powder via vacuum sintering and HIP treatments. *Materials Transactions*, 55: 1623-1629.
13. Chen, Q., Zhou, K., Jiang, L., Lu, Y., Li, T. (2015). Effects of Fe Content on Microstructures and Properties of AlCoCrFe_xNi High-Entropy Alloys. *Arabian Journal for Science and Engineering*, 40: 3657-3663.
14. Chen, S., Qiao, J., Diao, H., Yang, T., Poplawsky, J., Li, W., Meng, F., Tong, Y., Jiang, L., Liaw, P.K. et al (2023). Extraordinary creep resistance in a non-equiatomic high-entropy alloy from the optimum solid-solution strengthening and stress-assisted precipitation process. *Acta Materialia*, 244:118600.
15. Donachie, M.J. & Donachie, S.J. (2002). *Superalloys: A Technical Guide*, 2nd edition, ASM International, Materials Park.
16. Firstov, S.A., Rogul, T.G., Krapivka, N.A., Ponomarev, S.S., Kovylyayev, V.V., Danilenko, N.I., Bega, N.,D., Danilenko, V.I., Chugunova, S.I. (2016). Structural Features and Solid-Solution Hardening of High-Entropy CrMnFeCoNi Alloy. *Powder Metallurgy and Metal Ceramics*, 55: 225-235.
17. Galetz, M.C., Schlereth, C., White, E.M.H. (2021). Behavior of copper-containing high-entropy alloys in harsh metal-dusting environments. *Materials and Corrosion*, 72: 1232-1242.
18. Gui, W., Zhang, H., Yang, M., Jin, T., Sun, X., Zheng, Q. (2017). The investigation of carbides evolution in a cobalt-base superalloy at elevated temperature. *Journal of Alloys and Compounds*, 695: 1271-1278.

19. Gui, W., Zhang, X., Zhang, H., Sun, X., Zheng, Q. (2019). Melting of primary carbides in a cobalt-base superalloy. *Journal of Alloys and Compound*, 787: 152-157.
20. Gwalani, B., Gorsse, S., Soni, V., Carl, M., Ley, N., Smith, J., Ayyagari, A.V., Zheng, Y., Young, M., Mishra, R.S., et al (2019). Role of copper on L1₂ precipitation strengthened fcc based high entropy alloy. *Materialia*, 6:100282.
21. Ilyas, S., Ranjan Srivastava, R., Singh, V.; Chi, R., Kim, H. (2022). Recovery of critical metals from spent Li-ion batteries: Sequential leaching, precipitation, and cobalt-nickel separation using Cyphos IL104. *Waste Management*, 154: 175-186.
22. Jafari, A., Khorram, A., Boutorabi, S. M.A. (2018). Microstructure Evolution of MAR-M302 Superalloy During Heat Treatment at High Temperatures. *Transactions of the Indian Institute of Metals*, 71: 685-695.
23. Ji, W., Wu, M. (2022). Nanoscale origin of the crystalline-to-amorphous phase transformation and damage tolerance of Cantor alloys at cryogenic temperatures. *Acta Materialia*, 226:117639.
24. Kaypour, H., Nategh, S., Gholamipour, R., Khodabandeh, A. (2023). Effect of Aluminum Addition on Microstructure, Recrystallization and Work Hardening of MnCrCoFeNi High-Entropy Alloy. *Transactions of the Indian Institute of Metals*, 76:119-133.
25. Kofstad, P. (1988). *High temperature corrosion*, Elsevier applied science, London.
26. Kriese, F., Lassen, S., Niemeyer, B. (2023). Recovery process for critical metals: selective adsorption of nickel(II) from cobalt(II) at acidic condition and elevated temperature. *Adsorption Science & Technology*, 5334353.
27. Li, Q., Tian, S., Yu, H., Tian, N., Su, Y., Li, Y. (2015). Effects of carbides and its evolution on creep properties of a directionally solidified nickel-based superalloy. *Materials Science & Engineering, A: Structural Materials: Properties, Microstructure and Processing*, 633: 20-27.
28. Li, X.W., Wang, L., Dong, J.S., Lou, L.H. (2014). Effect of solidification condition and carbon content on the morphology of MC carbide in directionally solidified nickel-base superalloys. *Journal of Materials Science & Technology*, 30: 1296-1300.
29. Li, Y., Fu, H., Zhu, Z., Zhang, L., Li, Z., Li, H., Zhang, H. (2023). Effects of Fe/Ni Ratio on Microstructure and Properties of FeNiCrAlNb High-Entropy Alloys. *Advanced Engineering Materials*, 25: 2201686.
30. Liu, C., Jiang, H., Dong, J., Yao, Z., Niu, Y. (2020). Cold deformation mechanism of cobalt-base superalloy GH5605. *Materials Letters*, 267: 127533.
31. Lu, L., Ni, J., Zhao, D., Wang, C. (2021). Influence of Si and Mn on Solidification Characteristics and Mechanical Properties of a Ni-Based Superalloy. *Zhuzao*, 70: 52-60.
32. Lughofer, C., Tost, M. (2023). Lithium and Cobalt-Opportunities and Problems Regarding Two Critical Raw Materials in the EU. *Berg- und Hüttenmännische Monatshefte*, 186: 305-308.
33. Mukanov, S., Loginov, P., Fedotov, A., Bychkova, M., Antonyuk, M., Levashov, E. (2023). The Effect of Copper on the Microstructure, Wear and Corrosion Resistance of CoCrCuFeNi High-Entropy Alloys Manufactured by Powder Metallurgy. *Materials*, 16: 1178.
34. Oliveros, D., Fraczkiwicz, A., Dlouhy, A., Zhang, C., Song, H., Sandfeld, S., Legros, M. (2021). Orientation-related twinning and dislocation glide in cantor high entropy alloy at room and cryogenic temperature studied by in situ TEM straining. *Materials Chemistry and Physics*, 272:124955.
35. Pedrazzini, S., Child, D.J., West, G., Doak, S., Hardy, M.C., Moody, M.P., Bagot, P.A.J. (2016). Oxidation behaviour of a next generation polycrystalline Mn containing Ni-based superalloy. *Scripta Materialia*, 55: 8741-8755.
36. Qin, X.Z., Wang, J.Q., Cheng, S.H., Wu, Y.S., Zhou, L.Z. (2023). Evolution of microstructure and 800°C/294 MPa stress rupture property of cast Ni-based superalloys during long-term thermal exposure: Role and behavior of primary MC carbide. *Materials Science & Engineering, A: Structural Materials: Properties, Microstructure and Processing*, 881: 145416.
37. Razumov, N., Makhmutov, T., Kim, A., Masaylo, D., Kovalev, M., Popovich, A.

- (2023). Synthesis and properties of high-entropy CoCrFeNiMnW_x alloys. *Journal of Materials Research and Technology*, 24: 9216-9224.
38. Sathyanarayana R.CH.V., Venugopal, D., Srikanth, P.R., Lokeshwaran, K., Srinivas, M., Chary, C.J., Ashok Kumar, A. (2018). Effect of aluminum addition on the properties of CoCuFeNiTi high entropy alloys. *Materials Today: Proceedings*, 5:26823-26828.
39. Semiatin, S.L., Levkulich, N.C., Saurber, A.E., Mahaffey, D.W., Payton, E.J., Senkov, O.N. (2017). The Kinetics of Precipitate Dissolution in a Nickel-Base Superalloy. *Metallurgical and Materials Transactions A: Physical Metallurgy and Materials Science*, 48: 5567-5578.
40. Sims, C.T. &Hagel, W.C. (1972). *The Superalloys*, John Wiley and Sons, New York.
41. Smekhova, A., Kuzmin, A., Siemensmeyer, K., Abrudan, R., Reinholz, U., Buzanich, A.G., Schneider, M., Laplanche, G., Yusenkov, K.V. (2022). Inner relaxations in equiatomic single-phase high-entropy Cantor alloy. *Condensed Matter*, 1-31.
42. Sun, W., Qin, X., Guo, J., Lou, L., Zhou, L. (2015). Thermal stability of primary MC carbide and its influence on the performance of cast Ni-base superalloys. *Materials & Design*, 69: 81-88.
43. Thurston, Keli V.S., Gludovatz, B., Hohenwarter, A., Laplanche, G., George, E.P., Ritchie, R.O. (2017). Effect of temperature on the fatigue-crack growth behavior of the high-entropy alloy CrMnFeCoNi. *Intermetallics*, 88:65-72.
44. Wei, Z., Zhao, W., Zhou, J., Liu, C., Zheng, Z., Qu, S., Tao, C. (2015). Microstructure Evolution of K6509 Cobalt-base Superalloy for Over-temperature. *Procedia Engineering*, 99: 1302-1310.
45. Yin, Y., Kent, D., Tan, Q., Bermingham, M., Zhang, M. (2020). Spheroidization behaviour of a Fe-enriched eutectic high-entropy alloy. *Journal of Materials Science & Technology*, 51: 173-179.
46. Young, D.J. (2008). *High temperature oxidation and corrosion of metal*, Elsevier Corrosion Series, Amsterdam.
47. Zhao, K. (2014). Prediction of TCP phases in nickel-base superalloys. *Advanced Materials Research*, 941-944: 120-123.